

Synthesis of novel Al-doped SnO₂ nanobelts with enhanced ammonia sensing characteristics

Sudip K. Sinha^{1,2*}

¹Department of Metallurgical and Materials Engineering, Indian Institute of Technology, Kharagpur 721302, India

²High Learning Centre, Central Institute of Plastic Engineering and Technology, Bhubaneswar 751024, India

*Corresponding author. Tel: (+91) 9830076244; E-mail: sudipiitk@gmail.com

Received: 13 September 2014, Revised: 01 November 2014 and Accepted: 15 November 2014

ABSTRACT

Pure and Al-doped single-crystalline 1-D SnO₂ based nanostructures were synthesized via a catalyst free simple chemical vapour transport and condensation process in Ar/O₂ atmosphere. The crystalline structure, morphology and defect states of pure and Al-doped SnO₂ nanostructures have been investigated in detail. Incorporation of Al in the interstitial voids of tetragonal SnO₂ lattice is proved by investigating through various analytical techniques. Al doping in SnO₂ significantly increases its defect concentration as demonstrated by photoluminescence spectra. The PL spectra for pure and Al-loaded SnO₂ samples shows a less intense excitonic peak at ~384 nm in the UV region apart from the broad and intense yellow emission peak centred at around ~596 nm and a shallow peak at ~672 nm, respectively. For the development of stable and economically viable sensor modules for ammonia vapour detection, sensitivity at three different concentration of NH₃ vapours (25ppm, 50 ppm and 100 ppm) were investigated by varying the operating temperature (250–400 °C). The minimum sensitivity for Al-doped SnO₂ nanobelts was found to be 0.47 (at 25 ppm and 250 °C) and the maximum as 1.85 (at 100 ppm and 350 °C), which is 2-3 times higher than that for pure SnO₂ nanowire assemblies. Our results are found to be reproducible after cross examination by repeated observations. The response time (35–110 s), and recovery time (50–120 s) of our Al-doped SnO₂ nanostructured sensors, for different concentrations of NH₃ vapours, are equivalent or less if compared to those of available metal-oxide sensors in market. Copyright © 2015 VBRI press.

Keywords: Crystalline; tin oxide; nanostructure; chemical vapour transport.



Sudip Kumar Sinha received his B. E. degree in the department of Metallurgical Engineering from Jadavpur University in the year 2003. Later he did his M. Tech and M. S degree from Indian Institute of Technology, Kanpur and Washington State University in the year 2007 and 2009, respectively. He obtained his PhD degree at the Indian Institute of Technology, Kharagpur in the year 2014. Presently he is appointed as an Assistant Professor/Lecturer at CIPET, Bhubaneswar, India.

His major areas of research are based on metal oxide based nanostructured materials particularly in form of nanowires/nanobelts etc. and thin films for the development of sensors and transparent conducting oxides. He has five research papers to his credit. He has presented numerous research papers at National and International conferences and received accolades.

Introduction

Tin oxide is used as an exceptional material for fabricating solid state gas sensors owing to some of its fundamental chemical and physical properties [1, 2]. In the last few years, doped or virgin tin oxide based nanowires, nanobelts and nanorods have been successfully synthesized [3, 4] and used as novel gas sensing materials [5, 6]. One-dimensional

(1D) and quasi-one-dimensional (quasi-1D) nanostructures including nanotubes, nanowires, and nanoribbons have fascinated both intensive and extensive research, owing to their unique advantage arising from low dimensionality and use in novel nanodevices. Interestingly, the high surface to-volume ratios of these low-dimensional nanostructures are particularly useful for increasing their electrical properties due to the extremely sensitive surface chemical reactions. Since the SnO₂ surfaces play a pivotal role in device effectiveness, the structural arrangement, oxygen vacancies, electrical and electronic properties, and physi-absorption of various gases on SnO₂ single crystals as well as films have been studied extensively [2, 7, 8]. The sensing response of these low-dimensional nanostructures can also be drastically improved by adding calculated amount of impurities, defects and active species on their surface. It is known that dopants are significant for the formation of oxygen vacancies, and they also modify the electronic structure and band gap energy of metal oxides. However, the growth mechanism and sensing behaviour of doped SnO₂ one dimensional nanostructures has not much reported as compared to its undoped counterpart. Ammonia (NH₃) is a highly toxic colourless gas with a typical pungent odour. Moreover it is corrosive to the skin, eyes,

and lungs. The permissible exposure limits for ammonia in an eight-hour TWA (Time Weighted Average) of 25 ppm [9]. As low as 300 ppm NH₃ vapour could be extremely dangerous to human life and health. Therefore suitable safety measures and proper detection of this gas is essential every time and everywhere to avoid serious accidental injury or death. In this backdrop, detecting ammonia vapour is a crucial task of gas sensor research and technology, particularly when its concentration exceeds TLV (threshold limit value) of 25 ppm.

It is imperative to mention that there is serious dearth of literature on ammonia vapour sensing of metal-oxide nanostructures either in thin film or in nanostructure form. Recent reports based on indium tin oxide (ITO) thin film [10], Fe₂O₃/Carbon nanotube [11] or multilayer graphene [12] have shown reasonable improvements. Therefore, the research efforts must be more extensive in the field of ammonia sensors. In this connection, it would be worthwhile to mention that Al³⁺ could be sensibly incorporated into SnO₂ host lattice and substitute the Sn⁴⁺ atoms to enhance the concentration of oxygen vacancy and other defects. This eventually increases its overall sensitivity. There is no report available on the systematic study Al-doped SnO₂ low-dimensional nanostructures prepared by thermal-evaporation method for NH₃ vapour detection.

In this study, we report a facile route to deposit pure and single-crystalline SnO₂ nanowires and Al-doped SnO₂ nanobelts. The enhanced ammonia vapour sensing performance of the pure and doped nanostructures was attributed to oxygen vacancy which was the primary adsorption and catalytic centre in this gas-sensing response. This work demonstrates the drastic enhancement of the gas-sensing performance of doped SnO₂ nanostructures as compared to pure SnO₂ because of oxygen vacancies arising from Al-doping. Moreover, it gives an insight on the growth mechanism of these novel nanostructures and also proposes an oxygen-vacancy-dominated gas-sensing mechanism for SnO₂.

Therefore, based on the above mentioned advantages of structural simplicity, ease of operation, reasonable cost, and outstanding sensing properties, the studied materials suggests a potential in the field of high performance ammonia sensing applications.

Experimental

Materials and sample preparation methods

The undoped and Al-doped SnO₂ nanostructures were grown by thermal evaporation of Sn powders (99.99%) and the mixed powders of Sn (Sigma-Aldrich, USA, 99.9 % pure) and Al (Alcoa, Texas, USA, 99.9 % pure) maintaining a 4:1 weight ratio (Sn:Al). The powders were kept in an alumina boat which was inserted in the central heating zone of the quartz tube (40 mm inner diameter) of a customized horizontal tube furnace. A number of *p*-Si (100) wafers (Semiconductor Wafer Inc., Taiwan) with 10 mm x 10 mm dimension, were positioned in a separate crucible in the downstream end and used as substrates for the deposits. The sources were heated from room temperature to 950 °C and 1150 °C under ambient pressure for the pure and mixed (Sn/Al) powders, respectively. Ar-2% O₂ (supplier:

Tapaswi enterprise) gas was introduced as the carrier gas and the flow rates were fixed as 100 SCCM and 200 SCCM respectively, for the two materials. After one hour, white wool like deposits was formed on the substrates.

Materials characterization

X-ray diffraction spectroscopy (XRD) was used to characterize the crystallographic phase and doping effect of the as-deposited products. A Philips PANalytical X'Pert pro using CuK_α (λ= 1.542 Å) radiation in the grazing-incidence mode was used for this purpose. To characterize the morphology of the obtained materials and measure the size, shape and distributions, scanning electron microscope (FE-SEM, ZEISS) was used. The crystallographic structure, growth habits and elemental distribution of the nanostructures were further characterized with atomic resolution by means of TEM and HRTEM in a Tecnai G² 30ST (FEI) field emission operated at 200 kV with energy dispersive X-ray spectroscopy (EDS) attached to the TEM. For TEM and HRTEM characterization, the as-deposited samples were collected by scraping the nanostructures off of the substrate over carbon-coated copper grids.

Room-temperature photoluminescence (PL) measurements were recorded using a He-Cd laser as an excitation source operating at a wavelength of 325 nm with a grating monochromator (TRIAx 320) fitted with a photomultiplier. The gas sensors were fabricated following a process described elsewhere [13].

Gas sensing measurements

Ammonia sensing measurements were done using a static test system that includes polycarbonate desiccators of known volume (17.5 L). The concentrations of the target gases (25 ppm, 50 ppm and 100 ppm) were determined by injecting a measured volume of liquid through micropipette into the desiccators. The ammonia is then converted to its vapour state in approximately 5 min. The operating temperature of the sensors was varied from 250°C - 400 °C. The response (*S*) of a sensor for reducing gas (e.g. NH₃, H₂ etc. where R_{gas} < R_{air}) is defined as,

$$S = R_a/R_g, \quad (1)$$

Where, *R_a* and *R_g* are the steady state baseline electrical resistance of the sensor in dry air and in ammonia-air mixed gas, respectively. The sensing properties were measured by using a high precision sensor testing system consisting Agilent multimeter (U1252A) attached with Agilent data logger software installed in a computer while the ambient relative humidity (RH) was under 45 %. The sensor temperature was maintained by a constant voltage/current source (Keithley 228 A). Before every gas-sensing test the sensors were individually treated by supplying air at the particular operating temperature to attain a uniform base resistance of the samples.

The sensor response and recovery times of all the fabricated sensors is also calculated here. The response time (τ_{res}) is defined as the time the sensor resistance (conductance) takes to reach the 90% of its final value. The recovery time (τ_{rec}) is defined as the time the sensor response takes to recover the 70% of its baseline value.

Results and discussion

Phase analysis by XRD

The X-ray diffraction (XRD) patterns of pure and Al-doped SnO₂ nanostructures are shown in **Fig. 1**. The main peaks in the XRD plots correspond to the rutile structure of SnO₂ (JCPDF File # 41-1445). Apart from the SnO₂ diffraction peaks, orthorhombic alumina (Al₂O₃) peaks are also detected, indicating the oxidation of aluminium in the Al-doped SnO₂ nanostructured deposits. It is clearly seen in the diffraction plot of Al-doped SnO₂ deposits that the intensity of the peaks connected with the second phase is much lower compared to rutile SnO₂ phase. However, the presence of pure aluminium peak, in the Al-doped SnO₂ nanobelts indicates that some part of the powder mixture remains unreacted. The major diffraction peaks are observed from (110), (101), (200), (211) and (220) lattice planes from SnO₂ crystal in both the structures.

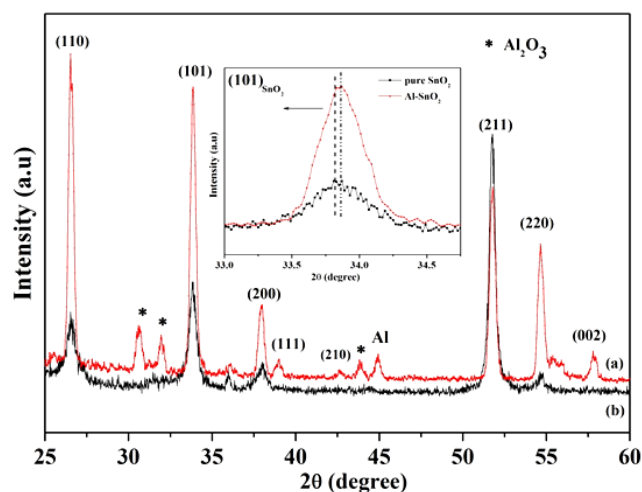


Fig. 1. X-ray diffraction patterns of as-synthesized Al-doped and inset: pure SnO₂ nanostructures.

As the covalent radius of Al (0.118 nm) is smaller than that of Sn (0.141 nm), incorporation of Al³⁺ at the interstitial position of SnO₂ sub-lattice leads to an increase of lattice parameter (*d*-value) and subsequent distortion of the SnO₂ host lattice. The 0.05° (*2θ*) peak shift of (101) plane of Al-doped SnO₂ nanobelts to the lower angle side of XRD plot (**Fig. 1** inset) with respect to undoped SnO₂ nanowires is an indication of this observation.

Surface morphology and growth mechanism

The morphology and structure of the as-synthesized nanostructures was observed by using TEM and SEM. **Fig. 2** (a) shows FESEM micrograph of Al-doped SnO₂ nanostructures. The Al-doped SnO₂ nanostructures deposited is mainly in the form of nanobelts in large amounts. However other morphologies, namely, nanowires and nanorods are also found minor amounts in the deposits. The doped SnO₂ nanobelts with novel morphology exhibit few tens to about several hundreds of nanometers in width and a few tens of micrometers in length. The pure SnO₂ nanostructures (Inset figure) were primarily deposited in

the form of nanowires. The size ratio is comparable with the doped SnO₂ nanobelts.

To further confirm the uniform presence of aluminium element in SnO₂ nanobelts, energy dispersive X-ray analysis (EDS) was performed. **Fig. 2** (c-e) shows the EDS elemental map exhibiting the distribution of Sn, Al and O elements on an isolated nanobelt with small nanoparticles attached with it while **Fig. 2** (b) shows the corresponding FESEM image.

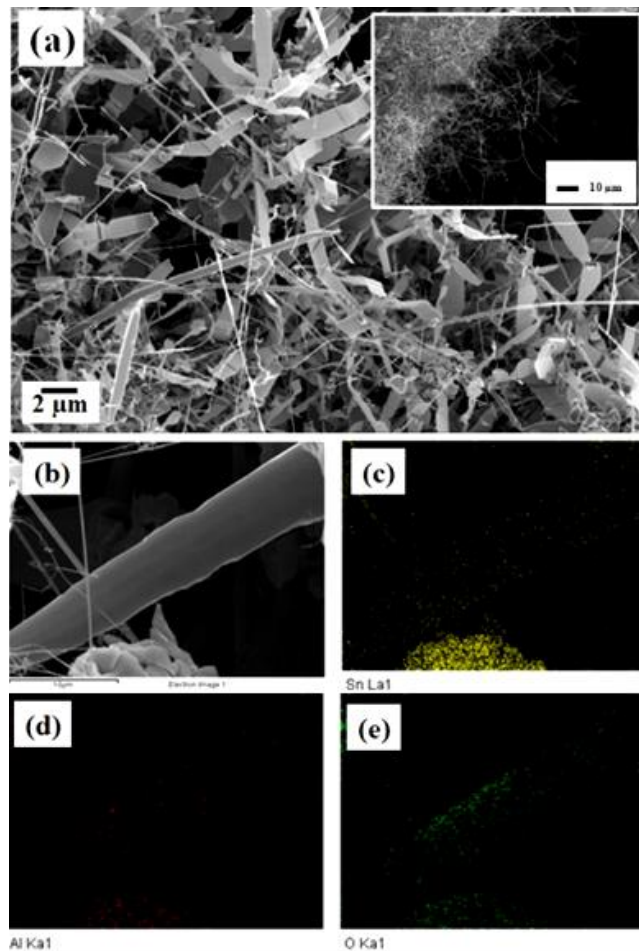


Fig. 2. (a) FESEM image of Al-doped SnO₂ nanobelt mesh. (Inset: Side view of pure SnO₂ nanowire network), (b) FESEM image of a single nanobelt taken for EDS analysis. EDS elemental maps showing distribution of (c) Sn, (d) Al and (e) O.

As no metal catalyst was used to synthesize the pure and Al-doped SnO₂ nanostructures, the conventional vapour-liquid-solid (VLS) model is not valid in the present case. We posit the “vapour-solid” (VS) mechanism to explain the growth of Al-doped SnO₂ nanobelts in the present case.

Pure tin has low melting point (232 °C) as compared to pure aluminium (660 °C). Although the boiling point of pure tin (2602 °C) is comparable with pure aluminum (2519 °C). In the reaction temperature regime (1100 °C) for Al-Sn powder mixtures, the saturation vapour pressure of metallic Sn is higher compared to metallic Al. As a result, the formation of SnO₂ whiskers as compared to Al₂O₃ whiskers is more energetically favourable. Accordingly, Sn melts, vapourize and forms its higher valence oxide earlier than Al. Moreover, incomplete or partial melting of Sn metal results in deposition of small amount of metallic Sn

in the surface of the nanostructures. The detailed crystallographic development of an individual nanobelt is investigated by HRTEM studies, as shown in **Fig. 3**. **Fig. 3 (a)** shows the typical TEM image of individual Al-doped SnO₂ nanobelt with its width ranging from 60 nm–200 nm, as the structure is not uniform width wise. Ripple-like contrast, which most often forms due to lattice strains, is not observed in the nanobelt structure. The clear lattice fringes of the HRTEM image (**Fig. 3 (b)**) as recorded from the highlighted region of the nanobelt indicate the formation of a perfect single crystalline SnO₂ structure.

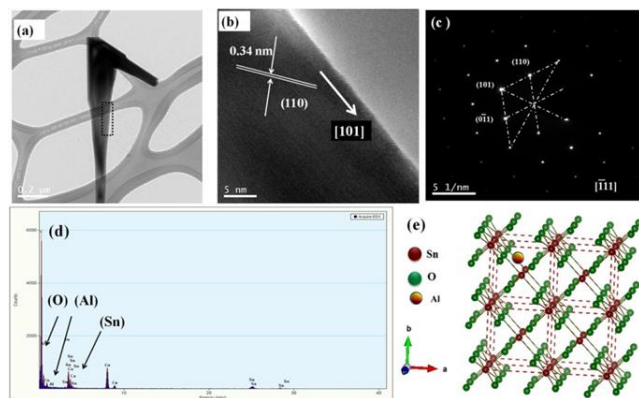


Fig. 3. (a) TEM image of a portion of Al-doped SnO₂ nanobelts (b) HRTEM image taken from the highlighted region of the TEM image (c) The corresponding SAED pattern properly indexed (d) EDS line scan showing presence of Sn, Al and O signal and (e) Tetragonal SnO₂ lattice indicating the presence of Al atom in the internal void.

The lattice spacing between two adjacent (110) planes is measured to be 0.34 nm, representing the growth of Al-doped rutile SnO₂ along the [101] direction. The corresponding selected area electron diffraction (SAED) pattern (**Fig. 3c**) is indexed as a tetragonal rutile SnO₂ single crystal (with [-111] zone axis) and it is in good agreement with our XRD findings. The EDX line scan analysis (**Fig. 3 (d)**) also reveals that the nanobelts are composed of three different elements Sn, O and Al. From the investigation of the XRD and TEM techniques, we predict that the Al atoms might be placed in the interstitial voids of SnO₂ lattice and eventually producing numerous lattice defects with no annihilation of the parent rutile phase of SnO₂ crystals. **Fig. 3e** shows the schematic crystal structure of rutile SnO₂ lattice with Al atoms located in its interstitial positions.

Ammonia sensing performance

The ammonia-sensing characteristics of pure and Al-doped SnO₂ nanostructures are investigated by varying the ammonia vapour concentration (25 ppm, 50 ppm, 100 ppm) and sensor operating temperature (250–400 °C). **Fig. 4 (a)** show the resistance transient of Al-doped SnO₂ nanobelts sensing element during sensing of ammonia vapour of 25 ppm, 50 ppm and 100 ppm concentrations at 300 °C. It is evident from the plot that increasing the ammonia concentration increases the sensitivity of doped SnO₂ nanostructures. Similar resistance transient pattern, but with smaller variation, has been found for undoped SnO₂ nanowires. It is essential to make a comparison of sensor

response between pure SnO₂ and Al metal-loaded SnO₂ nanostructured sensors.

Fig. 4 (b) shows the variation in sensitivity, with respect to change in ammonia vapour concentration for both pure and Al-doped SnO₂ nanostructures at 350 °C. It is shown that the gas response rapidly increases with increasing NH₃ vapour concentration. The bar chart also clearly indicates that the Al-doped SnO₂ nanobelts outperformed the undoped SnO₂ nanowires in terms of sensitivity and follows almost a linear growth pattern with increasing ammonia vapour concentrations, in either case. A closer look at the bar chart reveals that as high as two-fold enhancement in sensitivity is reached for various ammonia concentrations at this temperature if the SnO₂ are doped with Al³⁺. Similar results have been obtained for other working temperatures (i.e. 250 °C, 300 °C and 400 °C) also. These findings suggest that the Al-doped SnO₂ nanostructure is more favourable to detect NH₃ in the tested vapour concentration.

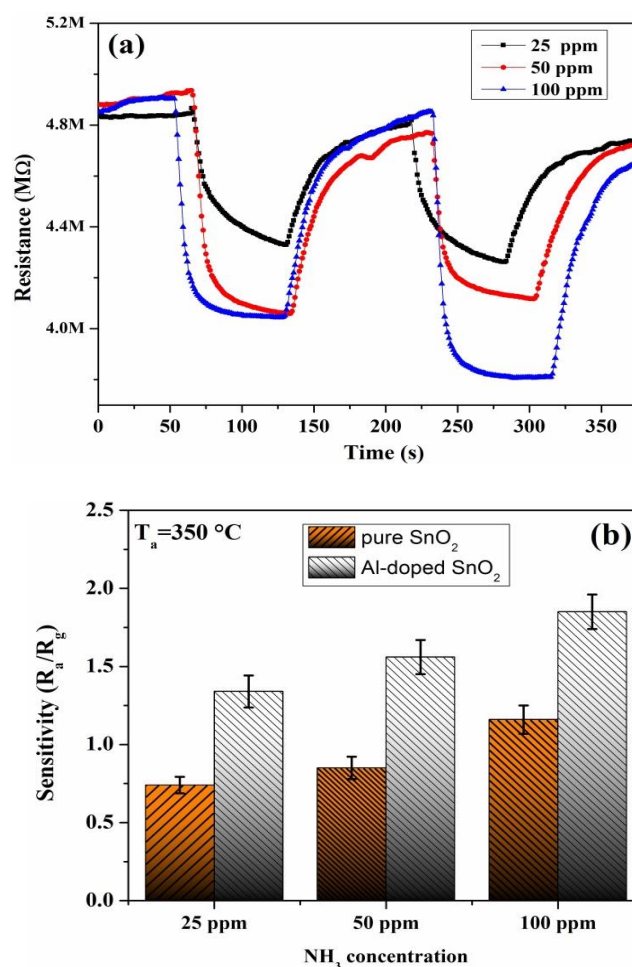


Fig. 4. (a) Typical response transients of the Al-doped SnO₂ nanobelt sensors in different ammonia vapour concentrations vapour at 300 °C and (b) Histogram showing a comparison in ammonia sensitivity between pure and Al-doped SnO₂ nanostructures at 350 °C with varying vapours concentration.

Fig. 5 shows the sensitivity of both the nanostructured sensors as a function of four different sensor operating temperature (250–400 °C) for 100 ppm of ammonia vapour. The temperature variations have the benefit to find an optimum operating temperature at which the sensitivity

will be highest for a particular concentration of analyte gas. It can be inferred from **Fig. 5**, that at lower operating temperature (250 °C) the sensitivity is almost same for the two different nanostructures. However, with increasing temperature, the sensitivity of the Al-doped SnO₂ nanostructures increases to a much greater extent. The optimum operating temperature was 350 °C for both this materials and the value of sensitivity at this temperature is found to be 1.85 and 1.16 for 100 ppm of ammonia vapour, respectively.

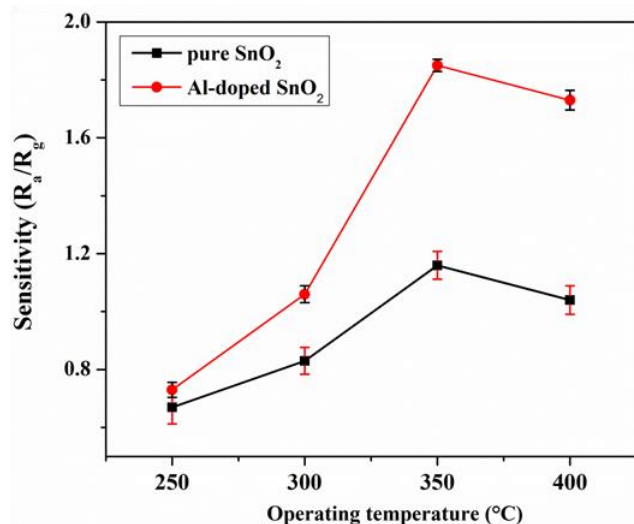
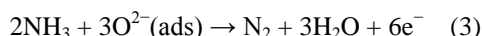


Fig. 5. Temperature modulation of the ammonia -sensing studies of the as deposited nanostructures in the presence of 100 ppm of test gas.

The response (τ_{res}) and recovery (τ_{rec}) times in presence of the test gas (i.e. NH₃), are found in the range of 60–130 s and 80–160 s for undoped SnO₂ nanostructures. The values of response and recovery time improved significantly for the Al-doped SnO₂ nanostructures and found in the range of 35–110 s and 50–120 s, respectively. Our results indicate much better ammonia sensitivity and sensor response and recovery times compared to previously reported results [14] for SnO₂ nanostructures in the identical concentration range.

Ammonia sensing mechanism

It is now known [15] that the oxidizing (e.g. NO₂, NO or CO₂ etc.) or reducing (e.g. H₂S, CO, NH₃, CH₄ etc.) gas-sensing mechanism of p-type or n-type semiconductor sensors is principally based on a variation in the electrical conductivity (or resistivity). When atmospheric O₂ is adsorbed on the surface of sensor materials, it eventually trap and react with the electrons from its surface to produce negatively charged oxygen species (ions), such as O₂⁻, O⁻, and O²⁻. Therefore, an electron depletion layer (space charge layer) forms near the surface, which increases the device resistance. Upon exposure to the device, the target gas (NH₃) reacts with ionic oxygen species, and the trapped electrons are released back to the conduction band of these nanostructured sensor materials, leading to an increase in conductivity or decrease in resistivity. The overall reducing reactions between NH₃ and the chemisorbed oxygen species can be depicted as follows:



The improved sensing performance of the Al-doped SnO₂ nanostructures as compared to the undoped counterpart is attributed by the formation of oxygen vacancies due to incorporation of Al atom the within the SnO₂ lattice.

Photoluminescence spectra

To explore any correlation between the structure of the specimens and their enhanced performance towards the test gas (NH₃), PL measurements were recorded as depicted in **Fig. 6**. Photoluminescence spectroscopy is often used for characterizing intrinsic defects in oxide semiconductors. In the PL spectra, the high intensity visible emission of the Al-doped SnO₂ nanostructures as compared to undoped one, gives an indication of abundant structural defects on the surface of the doped SnO₂ nanostructures.

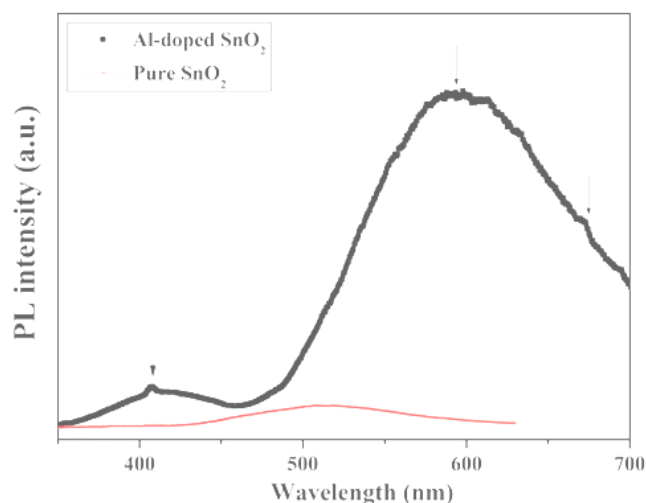


Fig. 6. Photoluminescence spectra of the pure and Al-doped SnO₂ nanostructures. The arrowheads indicate major PL peak positions.

The band-to-band emission (340 nm) for both the nanostructures was not observed in our samples. A less intense peak at ~384 nm in the UV region is found which is supposed to form due to recombination of excitonic centres [16]. Al-doped SnO₂ nanobelts shows a broad and intense visible yellow PL emission peak centred at around ~596 nm, and a shallow peak at 672 nm representing the orange emission. However, the pure SnO₂ nanowires exhibit only one green emission peak centred at 512 nm which is much less strong than the doped nanostructures. Lei et al. [17] have shown the formation of green and yellow emission band centred at 537 and 575 nm in the Al-doped SnO₂ nanowires due to lattice distortion arising from incorporation of Al atoms in the SnO₂ sublattice. The visible band which originates from the luminescence of trapped states associated with defects, for instance oxygen vacancies (V_O) or tin interstitials are generated during the entire growth process. It has been revealed that the yellow emission is associated with ionized oxygen vacancies (V_O), whereas the orange emission originates from the Sn interstitials (Sn_i) [18]. In Al-doped SnO₂ nanobelts, Al atoms take the interstitial position of the

SnO₂ crystal causing severe lattice distortion and incorporate lattice defects (most commonly O-vacancies). The various defects and O-vacancies in the SnO₂ lattice act as adsorption sites for oxygen. Consequently, the enhanced defect density in Al-doped SnO₂ nanostructures increase the sensitivity of doped nanostructures compared to the undoped SnO₂ nanostructures.

Conclusion

In summary, we have deposited pure and Al-doped SnO₂ 1-D nanostructures with wire and belt like morphologies by a simple catalyst free direct thermal evaporation technique and tested their reaction in various concentrations of NH₃ vapours. The incorporation of Al atoms within the SnO₂ lattice is envisaged by the lower angle shift of the XRD peak in the doped SnO₂ nanostructures, apart from usual FESEM-EDS analysis. The HRTEM lattice fringe image and corresponding SAED pattern of the Al-doped SnO₂ nanobelts indicates that the growth habit is dominated by [101] growth directions. The sensitivity of the as-prepared pure and Al-doped SnO₂ nanostructured sensors were measured at three different concentrations of NH₃ vapour (25ppm, 50 ppm and 100 ppm) with varying working temperatures (250–400 °C). It is found that in every case the doped nanostructures exhibit a much higher response to ammonia vapour as compared to the undoped SnO₂ nanowire arrays. The optimum operating temperature was found to be 350 °C in either case. The response (35–110 s) and recovery times (50–120 s) of the Al-doped SnO₂ nanostructured sensors are comparable or better to most of the available solid-state sensors for NH₃ detection in this concentration range. The sensing mechanism is dominated by the generation of new trapped centres and defects which are introduced into the SnO₂ lattice after Al doping, as evident from PL spectra. This reveals that the Al-doped SnO₂ nanostructures have the potential to use for detection of ammonia vapours at lower concentration levels.

Acknowledgements

This work was financially supported by the Department of Science and Technology, New Delhi, Indian National Academy of Engineering (Project: VVC) and Council of Scientific and Industrial Research (CSIR), Government of India. The author is grateful to CSIR-CGCRI for providing experimental facility for gas sensor set up. The use of VESTA open source software for constructing the crystal structure is gratefully acknowledged. Finally, the author would like to express his profound gratitude to Prof. I. Manna and Prof. S. K. Ray for their expert guidance to conduct this research work.

Reference

- Gopel W.; Schierbaum K.D.; *Sens. Actuators B* **1995**, *26*, 1.
DOI: [10.1016/0925-4005\(94\)01546-T](https://doi.org/10.1016/0925-4005(94)01546-T)
- Batzill M.; Diebold U.; *Prog. Surf. Sci.* **2005**, *79*, 47.
DOI: [10.1016/j.progsurf.2005.09.002](https://doi.org/10.1016/j.progsurf.2005.09.002)
- Pan Z.W.; Dai Z.R.; Wang Z.L.; *Science* **2001**, *291*, 1947.
DOI: [10.1126/science.1058120](https://doi.org/10.1126/science.1058120)
- Duan J. H.; Yang S.G.; Liu H.W.; Gong J.F.; Huang H.B.; Zhao X.N.; Zhang R.; Du Y.W.; *J. Am. Chem. Soc.* **2005**, *127*, 6180.
DOI: [10.1021/ja042748d](https://doi.org/10.1021/ja042748d)
- Comini E.; Faglia G.; Sberveglieri G.; Pan Z.W.; Wang Z.L.; *Appl. Phys. Lett.* **2002**, *81*, 1869.
DOI: [10.1063/1.1504867](https://doi.org/10.1063/1.1504867)
- Law M.; Kind H.; Messer B.; Kim F.; Yang P.D.; *Angew. Chem. Int. Ed.* **2002**, *41*, 2405.
DOI: [10.1002/1521-3773\(20020703\)41:13<2405::AID-ANIE2405>3.0.CO;2-3](https://doi.org/10.1002/1521-3773(20020703)41:13<2405::AID-ANIE2405>3.0.CO;2-3)
- Cox D.F.; Fryberger T.B.; Semancik S.; *Surface. Phys. Rev. B* **1988**, *38*, 2072.
DOI: [10.1103/PhysRevB.38.2072](https://doi.org/10.1103/PhysRevB.38.2072)
- Bergmayer W.; Tanaka I.; *Appl. Phys. Lett.* **2004**, *84*, 909.
DOI: [10.1063/1.1646460](https://doi.org/10.1063/1.1646460)
- Henderson R.; Ammonia spills in New York State HSEES, 1993-1998; (Eds.); Hazardous Substances Emergency Events Surveillance, New York State Dept. of Health, Bureau of Toxic Substance Assessment: Troy, N.Y., **2000**.
- Lin C.W.; Chen H.T.; Chen T.Y.; Huang C.C.; C.S. Hsu; Liu W. C.; *IEEE Trans. Electron Dev.* **2011**, *58*, 4407.
DOI: [10.1109/TED.2011.2167234](https://doi.org/10.1109/TED.2011.2167234)
- Muthukumar P.; Sumathi, C.; Wilson J.; Sekar, C.; Leonardi S. G.; Neri G. *Sensor Lett.* **2014**, *12*, 17.
DOI: [10.1166/sl.2014.3220](https://doi.org/10.1166/sl.2014.3220)
- Ghosh R.; Singh A.; Santra S.; Ray S.K.; Chandra A.; Guha P.K. ; *Sens. Actuators B: Chem.* **2014**, *205*, 67.
DOI: [10.1016/j.snb.2014.08.044](https://doi.org/10.1016/j.snb.2014.08.044)
- Das S.; Chakraborty S.; Parkash O.; Kumar D.; Bandyopadhyay S.; Samudrala S.K. ; Sen A.; Maiti H.S. *Talanta* **2008**, *75*, 385.
DOI: [10.1016/j.talanta.2007.11.010](https://doi.org/10.1016/j.talanta.2007.11.010)
- Meier D.C.; Semancik S; Button B.; Strelcov E.; Kolmakov A.; *Appl. Phys. Lett.* **2007**, *91*, 063118.
DOI: [10.1063/1.2768861](https://doi.org/10.1063/1.2768861)
- Duan J.; Gong J.; Huang H.; Zhao X.; Cheng G.; Yu Z.Z.; Yang S.; *Nanotechnology* **2007**, *18*, 055607.
DOI: [10.1088/0957-4484/18/5/055607](https://doi.org/10.1088/0957-4484/18/5/055607)
- Kar A.; Kundu S.; Patra A.; *J. Phys. Chem. C* **2011**, *115*, 118.
DOI: [10.1021/jp110313b](https://doi.org/10.1021/jp110313b)
- Lei M.; Hu Q.R.; Wang S.L.; Tang W.H.; *Mater. Lett.* **2010**, *64*, 19.
DOI: [10.1016/j.matlet.2009.09.058](https://doi.org/10.1016/j.matlet.2009.09.058)
- Gao T.; Wang T.H.; *Mater. Res. Bull.* **2008**, *43*, 836.
DOI: [10.1016/j.materresbull.2007.05.004](https://doi.org/10.1016/j.materresbull.2007.05.004)

Advanced Materials Letters

Publish your article in this journal

ADVANCED MATERIALS Letters is an international journal published quarterly. The journal is intended to provide top-quality peer-reviewed research papers in the fascinating field of materials science particularly in the area of structure, synthesis and processing, characterization, advanced-state properties, and applications of materials. All articles are indexed on various databases including DOI and are available for download for free. The manuscript management system is completely electronic and has fast and fair peer-review process. The journal includes review articles, research articles, notes, letter to editor and short communications.

